Heliyon 9 (2023) e17185

Contents lists available at ScienceDirect

Heliyon

journal homepage: www.cell.com/heliyon

High-temperature and stress response behavior of femtosecond laser pulses inscribed eccentric fiber Bragg gratings

Peng Jiang [a,b,c], Qiang Xu [a,b,c,*], Rui Zhang [a], Haiping Bai [d], Kang Li [e], Nigel Copner [e], Yongkang Gong [f]

[a] College of Physics and Optoelectronic Technology, Baoji University of Arts and Sciences, Baoji, 721016, China
[b] Engineering Technology Research Center for Ultrafast Optics and Advanced Material of Baoji, Baoji, 721016, China
[c] Baoji Key Laboratory of Micro-Nano Optoelectronics and Terahertz Technology, Baoji, 721016, China
[d] College of Science, Inner Mongolia Agricultural University, Hohhot, 010018, China
[e] School of Engineering, University of South Wales, Cardiff, CF37 1DL, United Kingdom
[f] School of Physics and Astronomy, Cardiff University, CF24 3AA, United Kingdom

ARTICLE INFO

Keywords:
Eccentric fiber Bragg gratings
Femtosecond laser
High temperature
Strain
Sensor

ABSTRACT

Eccentric fiber Bragg grating (EFBG) is inscribed in standard communication single-mode fiber using femtosecond laser pulses, and the temperature and strain sensing characteristics are experimentally demonstrated and analyzed. The EFBG exhibits strong thermal stability and good robustness in high-temperature measurement up to 1000 °C, and undergoes different thermal sensitivities during Bragg peak and the strong resonance coupled cladding spectral comb. The temperature sensitivity linearly increases with respect to the effective index of the resonant modes. Such a situation also occurs in axial strain measurement. These characteristics are of high interest for multiparametric sensing at high temperatures.

1. Introduction

Fiber grating sensor, due to its small size, corrosion resistance, anti-electromagnetic interference and good stability, can be applied in various engineering environments. Nowadays, it has been widely used in oil and gas chemical industry, civil engineering, aerospace and military fields [1,2]. By demodulating its transmitted optical signals, fiber grating sensor can sense a variety of external physical parameters such as temperature, strain, vibration, rotation, magnetic field and electric field [3–5]. In view of the needs of practical engineering, people put forward higher requirements for optical fiber sensors and no longer only focus on the single parameter measurement. Meanwhile, the cross interference between different physical parameter measurements will seriously affect the sensing performance of the system, so the importance of monitoring the sensing system with multiple parameters at the same time is also highlighted [6,7].

Eccentric fiber Bragg grating (EFBG) is birefringent grating, which is produced by using femtosecond pulses to induce highly localized refractive index modulation that deviates from the center of the fiber core [8–11]. In EFBGs, both the Bragg resonance and the cladding mode resonance are excited. Bragg resonance is inherently sensitive to ambient temperature and axial strain [12–14]. Meanwhile, cladding mode resonances has also been demonstrated to be applied to a variety of sensing, mainly for refractometric sensing [15–17], bending sensing [18–20]. Moreover, these femtosecond pulses fabricated gratings present very high thermal stability,

* Corresponding author. College of Physics and Optoelectronic Technology, Baoji University of Arts and Sciences, Baoji, 721016, China.
E-mail address: xuqiang@snnu.edu.cn (Q. Xu).

https://doi.org/10.1016/j.heliyon.2023.e17185
Received 9 November 2022; Received in revised form 8 June 2023; Accepted 9 June 2023
Available online 9 June 2023
2405-8440/© 2023 The Authors. Published by Elsevier Ltd. This is an open access article under the CC BY-NC-ND license (http://creativecommons.org/licenses/by-nc-nd/4.0/).

which can operate at temperatures higher than 1000 °C without any degradation [21,22]. These behaviors make EFBG a good potential platform for multiparametric sensing in harsh environments.

Temperature and strain are the two most important parameters in production safety and structural health monitoring. In this paper, we demonstrate the fabrication of EFBGs with the 800 nm fs laser pulses, then the thermal and stain characterization of EFBGs are investigated. The results show that the resonance wavelengths of EFBG increase linearly with temperature or axial strain. Meanwhile, we found that the Bragg and cladding resonant modes undergo different sensitivities, which linearly increases with respect to the effective index of the resonant modes. Based on that, potential multiparametric sensing of temperature and strain with EFBG is further illustrated.

2. Eccentric fiber Bragg gratings fabrication

Our EFBGs are fabricated by the point-by-point (PbP) writing technique using 800 nm fs pulses(100 fs width and 1 kHz repetition rate) delivered by amplified titanium-doped sapphire laser (Spectra-Physics) system. The experimental setup is shown in Fig. 1(a). The nonhydrogenated single-mode fiber (Corning SMF-28) is fixed on a high-precision accuracy, 3-dimensional nano-displacement platforms (Newport) with an accuracy of 5 nm. The vertical position of the fiber axis relative to laser focus (z-direction as shown in Fig. 1 (a)) could be visually controlled in reflection using a charge coupled device (CCD) positioned above the 100 × microscope objective lens. The visual process of writing fiber along the *x*-direction at a constant speed was monitored by the horizontal CCD. Using a broadband light source (NKT Photonics) as input light, the transmission spectra of EFBG are recorded by an optical spectrum analyzer (OSA, Yokogawa AQ6370). The attenuated irradiation energy in the fiber is estimated to be 1.5 μJ. Fig. 1(b) and (c) show the illustration and microscope image of the EFBG.

To fabricate EFBG, the fiber was shifted 2 μm off-center in the y direction and translated in the x direction at speed related to the desired period. Fig. 2 shows the amplitude spectra of a fourth-order EFBG with a period (Λ) of 2.144 μm. It can be seen that the Bragg resonance (λ_B) occurs at 1560.7 nm, and the comb-like amplitude spectrum of several hundred narrow-band cladding mode resonances occur on the left. The EFBG's main features are summarized in Table 1. Fig. 2 insert shows the comparison of cladding mode coupling between eccentric FBG and well-centered normal FBG. It is obvious that there are much stronger cladding mode coupling in EFBG.

3. Sensing mechanism of EFBGs

The Bragg resonance wavelength of the EFBGs can be denoted by the phase matching conditions as shown in equation (1) [14]:

$$m\lambda_B = 2n_{eff,core} \cdot \Lambda \tag{1}$$

and the resonance wavelength of the *j*th-order cladding mode can be expressed as shown in equation (2):

$$m\lambda_C^j = \left(n_{eff,core} + n_{eff,clad}^j\right) \cdot \Lambda \tag{2}$$

where $n_{eff,core}$ is the effective index of the core mode, $n_{eff,clad}^j$ is the effective index of the *j*th-order cladding mode, and the Λ is the grating period.

Considering only the environment temperature dT changes, the Bragg wavelength differential $d\lambda_B$ and the *j*th-order cladding mode wavelength differential $d\lambda_C^j$ can be written as following equations (3) and (4) [14]:

$$\frac{md\lambda_B}{dT} = 2\left(n_{eff,core} \cdot \frac{\partial \Lambda}{\partial T} + \Lambda \cdot \frac{\partial n_{eff,core}}{\partial T}\right) \tag{3}$$

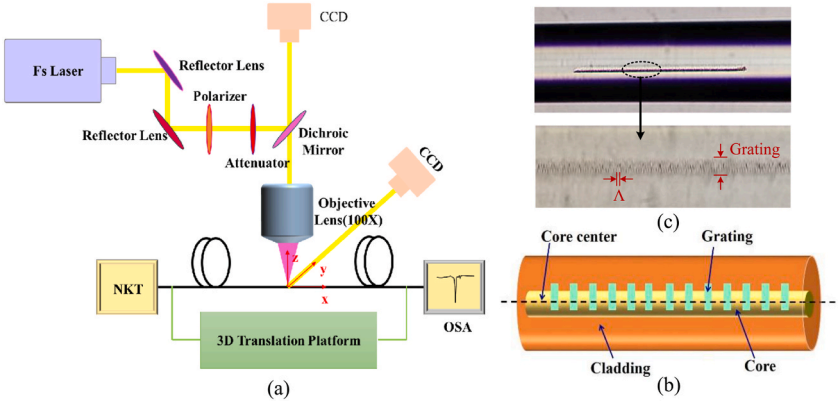

Fig. 1. (a) Experimental setup for fabricating EFBG. (b) Illustration and (c) microscope image of the EFBG.

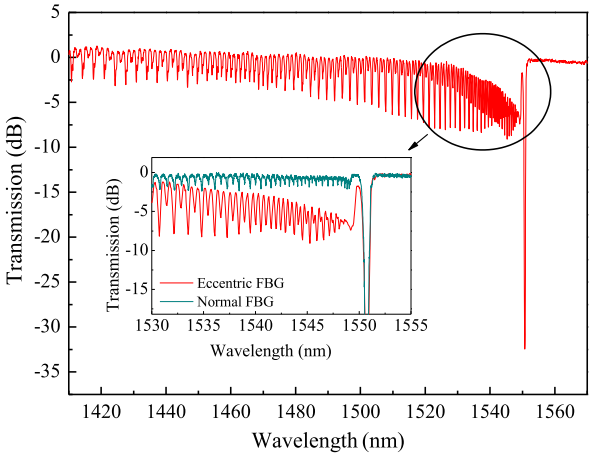

Fig. 2. Amplitude spectrum of an EFBG with Λ = 2.144 μm and L = 0.5 cm. Inset: zoomed contrast spectra of eccentric FBG and normal FBG.

Table 1
Main preparation parameters of EFBG.

Features	Data
Off-center	2 μm
Period	2.144 μm
Order:m	4
Length	5 mm
Bragg wavelength	1550.7 nm

$$\frac{md\lambda_C^j}{dT} = \left(\frac{\partial n_{\text{eff,core}} + \partial n_{\text{eff,clad}}^j}{\partial T}\right) \cdot \Lambda + \frac{\partial \Lambda}{\partial T} \cdot \left(n_{\text{eff,core}} + n_{\text{eff,clad}}^j\right) \tag{4}$$

The expression of equation (4) can also be transformed into the following equation (5):

$$\frac{md\lambda_C^j}{dT} = \left(n_{\text{eff,core}} \cdot \xi_{\text{core}} + n_{\text{eff,clad}}^j \cdot \xi_{\text{clad}}\right) \cdot \Lambda + \alpha \cdot \left(n_{\text{eff,core}} + n_{\text{eff,clad}}^j\right) \cdot \Lambda \tag{5}$$

where the $\xi_{\text{core}} = \frac{1}{n}\frac{\partial n_{\text{eff,core}}}{\partial T}$ and $\xi_{\text{clad}} = \frac{1}{n}\frac{\partial n_{\text{eff,clad}}^j}{\partial T}$ are respectively the thermo-optic coefficient of the core and cladding. The $\alpha = \frac{1}{\Lambda}\frac{\partial \Lambda}{\partial T}$ is the thermal expansion coefficient of the fiber waveguide.

When fiber is subjected to axial strain, a longitudinal displacement ΔL appears along the axial direction, which results in the change of grating period $\Delta\Lambda$. Within the linear elastic range, the axial strain ε of the grating is defined by equation (6) [23]:

$$\varepsilon = \frac{\Delta L}{L} = \frac{\Delta \Lambda}{\Lambda} \tag{6}$$

The Bragg wavelength differential $d\lambda_B$ and the jth-order cladding mode wavelength differential $d\lambda_C^j$ corresponding to axial strain in amplitude spectrum can be given by following equations (7) and (8) [24]:

$$\frac{md\lambda_B}{d\varepsilon} = 2\left(n_{\text{eff,core}} \cdot \frac{\partial \Lambda}{\partial \varepsilon} + \Lambda \cdot \frac{\partial n_{\text{eff,core}}}{\partial \varepsilon}\right) \tag{7}$$

$$\frac{md\lambda_C^j}{d\varepsilon} = \Lambda \frac{d\lambda_C^j}{d\varepsilon}\left(1 + \frac{\eta_{\text{core}} n_{\text{eff,core}} + \eta_{\text{clad}} n_{\text{eff,clad}}^j}{n_{\text{eff,core}} + n_{\text{eff,clad}}^j}\right) \tag{8}$$

where η_{core} and η_{clad} are respectively the elastic-optic coefficient of the core and cladding of the fiber. Therefore, Bragg wavelength and the jth-order cladding mode wavelength can be well used to monitor the longitudinal displacement.

In general, considering the combined action of strain and temperature, the resonant wavelength change of the fiber grating can be expressed as shown in equation (9) [25]:

$$\Delta\lambda(T, \varepsilon) = K_\varepsilon \Delta\varepsilon + K_T \Delta T \tag{9}$$

In the above relation, the cross term of thermal and strain response is ignored. As a result, for two resonant wavelengths to be

measured, the following equation holds:

$$\begin{bmatrix} \Delta\lambda_1 \\ \Delta\lambda_2 \end{bmatrix} = \begin{bmatrix} K_{\varepsilon 1} & K_{T1} \\ K_{\varepsilon 2} & K_{T2} \end{bmatrix} \begin{bmatrix} \Delta\varepsilon \\ \Delta T \end{bmatrix} \tag{10}$$

where K_ε and K_T are the temperature and strain sensitivities of EFBG, respectively. By measuring the variation of resonant wavelength with temperature and strain separately, the elements of the sensitivities matrix K can be determined experimentally. Once the sensitivity coefficient is calibrated by experiment, the applied strain and temperature change can be deduced.

4. Sensing experiments and discussions

For thermal characterization, the EFBG was placed in a heating furnace (Type: OTF-1200X) in its natural state (keep tension free). It should be noted that the EFBG had been annealed at 1050 °C for 4 h firstly before temperature behavior being measured. The wavelength and reflectivity of the grating would change slightly after the first high-temperature annealing. As shown in Fig. 3, the resonant wavelength decreases 0.92 nm and the amplitude increases by 4.4 dB when the temperature is cooled to room temperature after the first annealing. This can be explained as the refractive index change Δn with low stability (type I FBG) caused by scattering around the focus of femtosecond pulses can be erased during the high annealing process, which leads to the increase of modulation refractive index Δn_{mod} and the decrease of effective index Δn_{eff} [26].

Fig. 4(a) depicts the amplitude spectra of the EFBG under different furnace temperatures, which was increased from 25 °C to 1000 °C at a rate of 20 °C/min. Every spectral data was recorded after 30 min of temperature stabilization. The furnace temperature accuracy is ±0.1 °C. In addition, repeated heating and cooling processes were recorded and the consistent amplitude spectra were obtained, indicating that the EFBG has strong thermal stability and good repeatability in high temperature.

In order to analyze each mode separately, we amplified the Bragg resonant peak (shown in Fig. 4(b)) and cladding resonant peak (shown in Fig. 4(c)) against different temperatures. We can see the Bragg wavelength and cladding mode resonant wavelengths both redshift with temperature increasing, but the wavelength shifts are not identical. During the process of increasing temperature, the resonant Bragg wavelength red-shifted about 14.03 nm. The top part of Fig. 5 shows the experimental and linear fitting results of the Bragg resonant wavelength. In which, the mean Bragg resonant temperature sensitivity is $K_{T,\,B} = 14.4$ p.m./°C with the R-squared of 0.999.

The bottom part of Fig. 5 illustrates the evolution of the thermal sensitivity of resonances located around selected wavelength in the amplitude spectra of EFBG. Be noted that the inscribing of EFBG destroys the cylindrical symmetry of fiber and creates birefringence locally, which results in resonance splittings between both polarization modes (radial and azimuth polarization modes) and is spectrally manifested by the splitting of higher-order mode resonant peaks. These modes may result in two adjacent resonance dips in the spectrum and have sensitivities with slight difference [9]. In our experiment, the sensitivity data is recorded by the resonances with deeper dip. From the experimental data, the shorter the wavelength of cladding mode (higher order), the lower the sensitivity. The temperature sensitivity K_T is approximately linear with the selected resonant wavelength λ_{res}. For the EFBG used in the experiment, the linear fitting relationship is $K_T = -4.770 + 0.0124\ \lambda_{res}$.

Equation (5) suggests that the wavelength temperature sensitivity is mainly related to the thermal-optic effect and thermal expansion effect of EFBG. The thermal-optic coefficient is directly related to the mode effective refractive index n^j_{eff}. According to equations (1) and (2), the resonant wavelength also corresponds to n^j_{eff}. Therefore, the relationship between temperature sensitivity and mode effective refractive index can be further expressed as $K_T = 4.844 + 6.646\ n^j_{eff}$.

In order to study the strain sensing performance, the EFBG was fixed at one end and the other end was hung with axial load, which added 40 g each time until to 260 g. It takes 10 min to establish the equivalent force after loading.

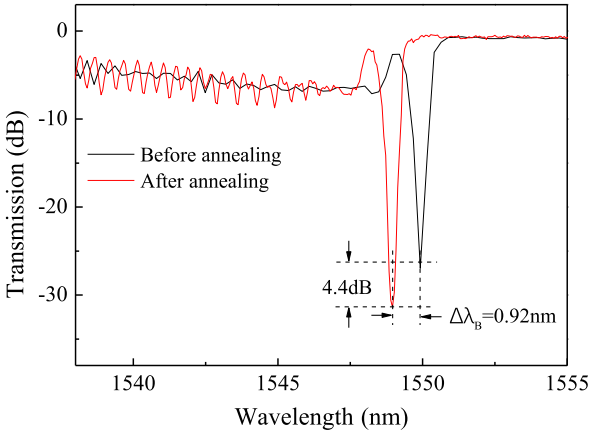

Fig. 3. Amplitude spectra of the EFBG before and after annealing at room temperature (25 °C).

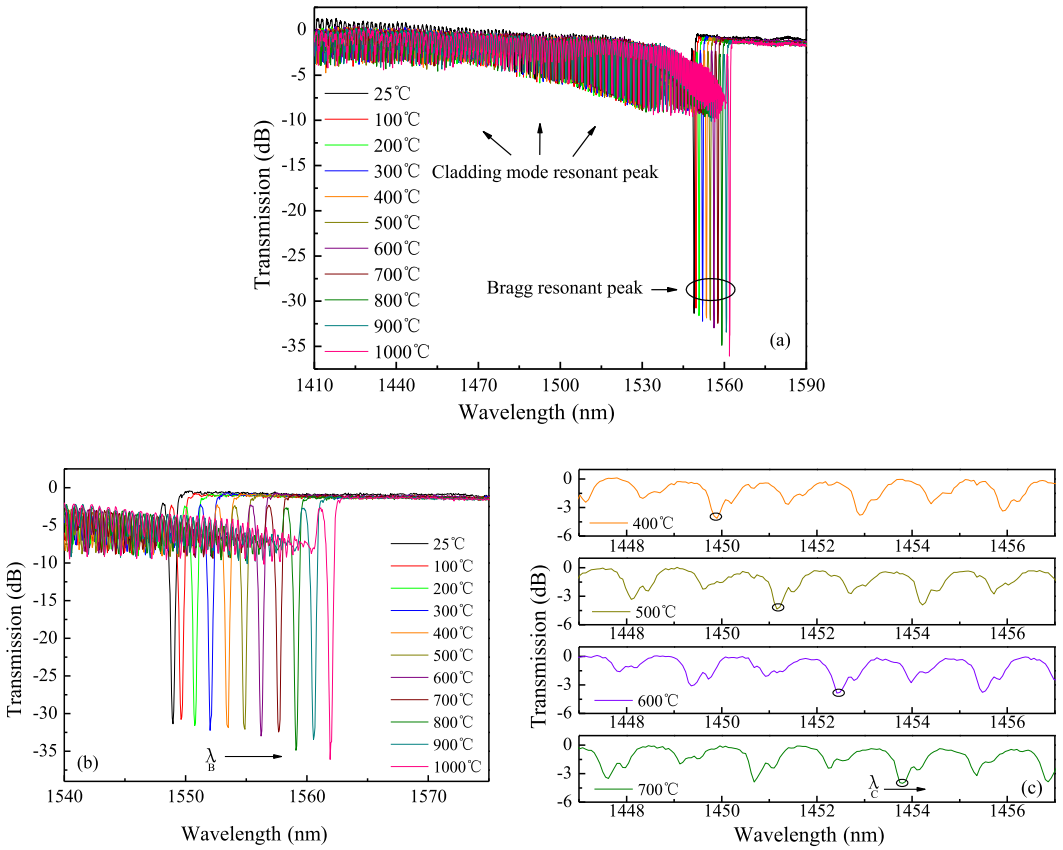

Fig. 4. (a) Amplitude spectra of the EFBG under different temperatures. Behaviors of the Bragg resonance (b) and the cladding resonance (c) with respect to temperature changes.

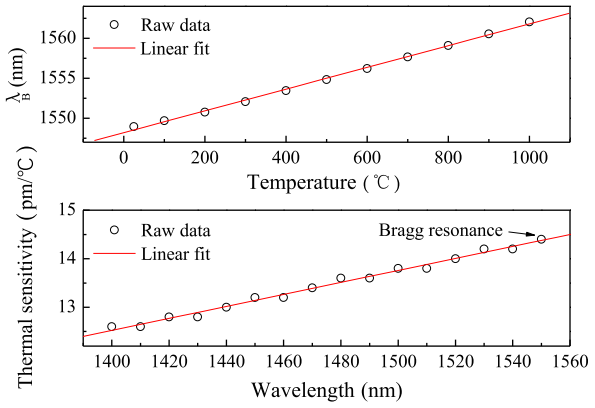

Fig. 5. Bragg wavelength shift with temperature (top) and thermal sensitivity of resonances located around selected wavelength in the amplitude spectra of EFBG (bottom).

The axial strain can be calculated from the load weight according to Hooke's law $\varepsilon = F/SY$. Where ε is axial strain, $Y = 7 \times 10^{10}$ N/m^2 is the Young's modulus of fiber, F is the axial tension, and S is the cross-sectional area of the fiber. Fig. 6(a) shows the amplitude spectra of a EFBG under different axial strains. In Fig. 6(b) and (c), we respectively amplified the Bragg resonant peak and cladding resonant peak for different applied axial strain. The experimental data show that the Bragg peak and cladding resonant wavelengths redshift when the axial strain increases. Similar to temperature response, these modes undergo different sensitivities. The top part of Fig. 7 depicts the linear regression of the experimental data for the Bragg peak, presenting a sensitivity of $K_{\varepsilon,\,B} = 1.15$ p.m./με with the R-squared of 0.999. The bottom part of Fig. 7 illustrates the evolution of the strain sensitivity of resonances located around selected wavelength in the amplitude spectra of EFBG. The strain sensitivity K_ε is approximately linear with the selected resonant wavelength

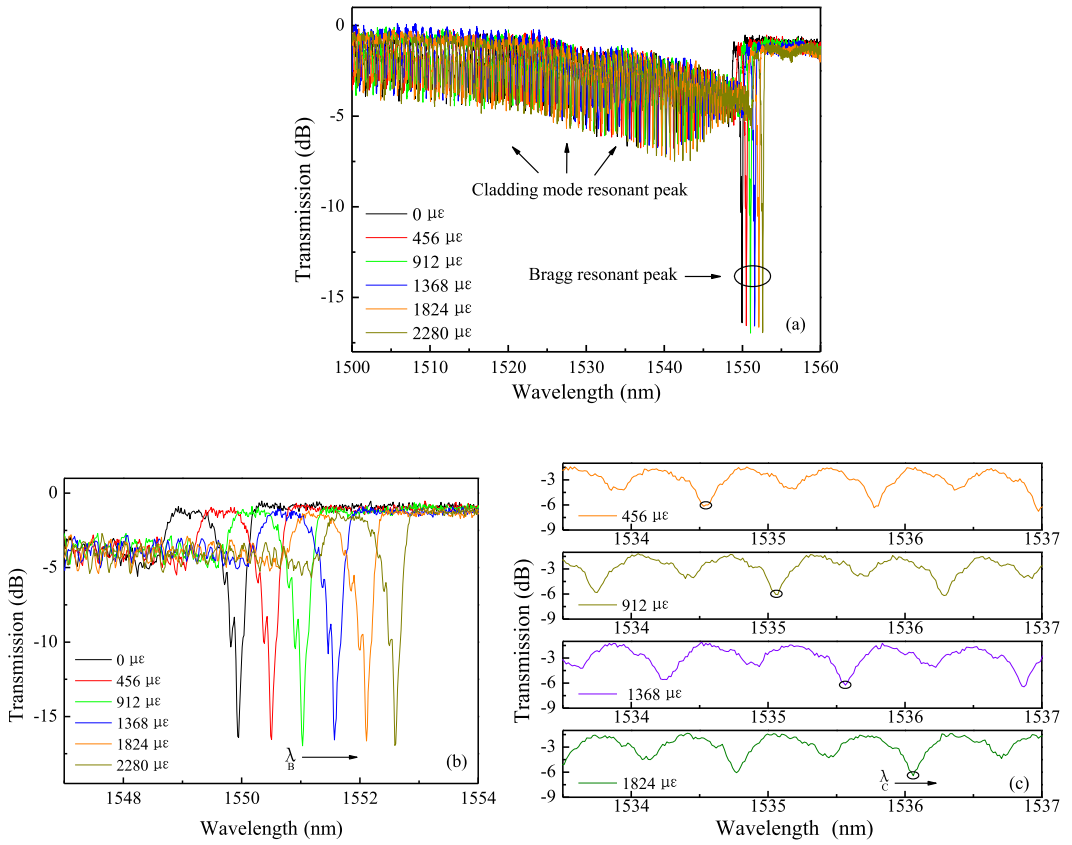

Fig. 6. (a) Amplitude spectra of a EFBG under different axial strains. Behaviors of the Bragg resonance (b) and the cladding resonance (c) with respect to axial strain.

λ_{res}., and the linear fitting relationship is $K_\varepsilon = -2.742 + 0.0025\lambda_{res}$. Similarly, the relationship between strain sensitivity and mode effective refractive index can be further expressed as $K_\varepsilon = -0.811 + 1.335\, n_{eff}^{j}$.

Based on the different behaviors of Bragg resonance and cladding resonance in spectra, multiparametric sensing can be realized by selective tracking of Bragg peak λ_B and cladding resonance peak λ_C. According to equation (10), temperature and strain can be determined simultaneously by decoupling processing, employing the following relationship:

$$\begin{bmatrix} \Delta T \\ \Delta\varepsilon \end{bmatrix} = \begin{bmatrix} K_{\varepsilon,B} & K_{T,B} \\ K_{\varepsilon,C} & K_{T,C} \end{bmatrix}^{-1} \begin{bmatrix} \Delta\lambda_B \\ \Delta\lambda_C \end{bmatrix} \tag{11}$$

where $\Delta\lambda_B$, $\Delta\lambda_C$ are wavelength shifts of Bragg and selected cladding resonance, $K_{\varepsilon,B}$ and $K_{\varepsilon,B}$ are temperature and strain sensitivitie of Bragg resonance, $K_{\varepsilon,C}$ and $K_{\varepsilon,C}$ are temperature and strain sensitivitie of selected cladding resonance, respectively.

The temperature and axial strain can be determined independently provided that the corresponding sensitivity satisfy the good conditions of the matrix inversion as indicated in equation (12):

$$D = K_{\varepsilon,B} \cdot K_{T,C} - K_{\varepsilon,C} \cdot K_{T,B} \neq 0 \tag{12}$$

According to the sensitivity extracted above, it can be calculated that the satisfied range covers the full resonant region of EFBG. So the two parameters of temperature and strain can be measured simultaneously according to equation (11).

5. Conclusion

In summary, the EFBG was successfully inscribed in nonhydrogenated standard communication fiber using femtosecond laser pulses with PBP direct writing technology. The sensing properties of the EFBG to temperature and axial strain were studied systematically. The grating presents a strong robustness for high temperatures up to 1000 °C with the Bragg sensitivity of 14.4 p.m./°C. For cladding mode resonance, the temperature sensitivity varies with the mode effective refractive index n_{eff}^{j}, the linear relationship can be written as $K_T = 4.844 + 6.646\, n_{eff}^{j}$. We also experimentally demonstrate that the resonant wavelength of the EFBG are linear to the axial strain, and in the cladding spectral comb the stain sensitivity decreases with the decrease of resonant wavelength. The

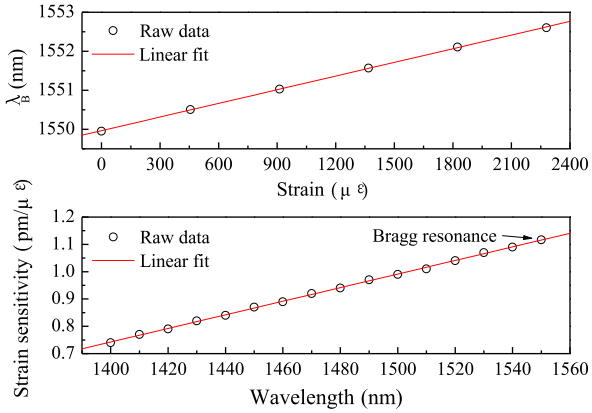

Fig. 7. Bragg wavelength shift with axial strain (top) and strain sensitivity of resonances located around selected wavelength in the amplitude spectra of EFBG (bottom).

sensitivities of the Bragg resonant peak is 1.15 p.m./με and the relationship between the strain sensitivity and n^j_{eff} can be expressed as $K_\varepsilon = -0.811 + 1.335\, n^j_{\text{eff}}$. These properties make EFBG a good potential platforms for multiparametric sensing in harsh environments.

Author contribution statement

Peng Jiang, Qiang Xu: Conceived and designed the experiments; Analyzed and interpreted the data; Wrote the paper.
Rui Zhang, Haiping Bai: Performed the experiments; Analyzed and interpreted the data.
Kang Li, Nigel Copner, Yongkang Gong: Contributed reagents, materials, analysis tools or data.

Data availability statement

Data will be made available on request.

Declaration of competing interest

The authors declare that they have no known competing financial interests or personal relationships that could have appeared to influence the work reported in this paper.

Acknowledgements

This work is supported by the International Science and Technology Cooperation and Exchanges Project of Shaanxi (Project No: 2021KW-39), Scientific Research Program Funded by Shaanxi Provincial Education Department (Project No: 22JC002) and Key Science and Technology Program of Shaanxi Province (Project No: 2023-YBGY-370), and Undergraduate Training Program for Innovation and Entrepreneurship of Baoji University of Arts and Sciences (Project No: 2021XJ112).

References

[1] G. Hegde, M. Prasad, S. Asokan, Temperature compensated diaphragm based Fiber Bragg Grating (FBG) sensor for high pressure measurement for space applications, Microelectron. Eng. 248 (2021), 111615.
[2] S. Alamandala, R. Prasad, R.K. Pancharathi, et al., Study on bridge weigh in motion (BWIM) system for measuring the vehicle parameters based on strain measurement using FBG sensors, Opt. Fiber Technol. 61 (3) (2021), 102440.
[3] F. Yang, W. Zhang, Q. Liu, et al., Silicon-microring-based interrogator for TDM-FBG sensors enabled by pulse compression, Opt. Lett. 45 (23) (2020) 6402.
[4] J. Frieden, J. Cugnoni, J. Botsis, et al., Vibration-based characterization of impact induced delamination in composite plates using embedded FBG sensors and numerical modelling, Compos. B Eng. 42 (4) (2011) 607–613.
[5] J.D. Lopez, A. Dante, C.C. Carvalho, et al., Simulation and experimental study of FBG-based magnetic field sensors with Terfenol-D composites in different geometric shapes, Measurement 172 (2021), 108893.
[6] X. Hui, W.X. Ren, Z.C. Wang, Deflection estimation of bending beam structures using fiber Bragg grating strain sensors, Adv. Struct. Eng. 18 (3) (2015) 395–404.
[7] G. Pereira, M. Mcgugan, L.P. Mikkelsen, Method for independent strain and temperature measurement in polymeric tensile test specimen using embedded FBG sensors, Polym. Test. 50 (2016) 125–134.
[8] C. Koutsides, K. Kalli, D. Webb, L. Zhang, Characterizing femtosecond laser inscribed Bragg grating spectra, Opt Express 19 (2011) 342–352.
[9] J. Thomas, N. Jovanovic, R. Becker, et al., Cladding mode coupling in highly localized fiber Bragg gratings II: complete vectorial analysis, Opt Express 20 (2012) 21434–21449.
[10] K. Chah, D. Kinet, M. Wuilpart, et al., Femtosecond-laser-induced highly birefringent Bragg gratings in standard optical fiber, Opt. Lett. 38 (2013) 594–596.
[11] K. Chah, V. Voisin, D. Kinet, et al., Surface plasmon resonance in eccentric femtosecond-laser-induced fiber Bragg gratings, Opt. Lett. 39 (2014) 6887–6890.
[12] Z. Wu, Y. Liu, Z. Wang, et al., Simultaneous measurement of curvature and strain based on fiber Bragg grating in two-dimensional waveguide array fiber, Opt. Lett. 38 (2013) 4070–4073.

[13] C. Li, T. Ning, J. Li, et al., Simultaneous measurement of refractive index, strain, and temperature based on a four-core fiber combined with a fiber Bragg grating, Opt Laser. Technol. 90 (2017) 179–184.
[14] H. Chikh-bled, K. Chan, Á. González-vila, et al., Behavior of femtosecond laser-induced eccentric fiber Bragg gratings at very high temperatures, Opt. Lett. 41 (2016) 4048–4051.
[15] H. Chikh-Bled, M. Debbal, M. Chikh-Bled, et al., Refractive index sensor in eccentric fiber Bragg gratings using a point-by-point IR femtosecond laser, Appl. Opt. 58 (2019) 528.
[16] Y. Jing, C. Guan, P. Tian, et al., In-fiber refractive index sensor based on single eccentric hole-assisted dual-core fiber, Opt. Lett. 42 (2017) 4470.
[17] C. Caucheteur, D. Paladino, P. Pilla, et al., External refractive index sensitivity of weakly tilted fiber Bragg gratings with different coating thicknesses, IEEE Sensor. J. 8 (2008) 1330–1335.
[18] C. Waltermann, A. Doering, M. Khring, et al., Cladding waveguide gratings in standard single-mode fiber for 3D shape sensing, Opt. Lett. 40 (2015) 3109–3112.
[19] W. Bao, Q. Rong, F. Chen, et al., All-fiber 3D vector displacement (bending) sensor based on an eccentric FBG, Opt Express 26 (2018) 8619.
[20] D. Su, X. Qiao, F. Chen, et al., Higher order coupling mode for orientation-dependent bend measurement using an off-Axis FBG inscription over few-mode fiber, IEEE Sens 18 (2018) 1368–1372.
[21] D. Grobnic, C. Smelser, S. Mihailov, R. Walker, Long-term thermal stability tests at 1000 °C of silica fibre Bragg gratings made with ultrafast laser radiation, Meas. Sci. Technol. 17 (2006) 1009–1013.
[22] J. He, Y. Wang, C. Liao, et al., Negative-index gratings formed by femtosecond laser overexposure and thermal regeneration, Sci. Rep. 6 (2016), 23379.
[23] R. Sante, L. Donati, Strain monitoring with embedded Fiber Bragg Gratings in advanced composite structures for nautical applications, Measurement 46 (2013) 2118–2126.
[24] M. Xu, J. Archambault, L. Reekie, et al., Discrimination between strain and temperature effects using dual-wavelength fiber grating sensors, Electron. Lett. 30 (1994) 1085–1087.
[25] S. Triollet, L. Robert, E. Marin, et al., Discriminated measures of strain and temperature in metallic specimen with embedded superimposed long and short fibre Bragg gratings, Meas. Sci. Technol. 22 (2011), 015202.
[26] L. Sudrie, M. Franco, B. Prade, , et al.A. Mysyrowicz, Study of damage in fused silica induced by ultra-short IR laser pulses, Opt Commun. 191 (2010) 333–339.